BNL-216188-2020-JAAM

Controlling Surface Phase Transition and Chemical Reactivity of O3-Layered Metal Oxide Cathodes for High-Performance Na-Ion Batteries

J. Song, E. Hu

To be published in "Journal of the American Chemical Society"

April 2020

Chemistry Department

Brookhaven National Laboratory

U.S. Department of Energy

USDOE Office of Energy Efficiency and Renewable Energy (EERE), Vehicle Technologies Office (EE-3V)

Notice: This manuscript has been authored by employees of Brookhaven Science Associates, LLC under Contract No. DE-SC0012704 with the U.S. Department of Energy. The publisher by accepting the manuscript for publication acknowledges that the United States Government retains a non-exclusive, paid-up, irrevocable, world-wide license to publish or reproduce the published form of this manuscript, or allow others to do so, for United States Government purposes.

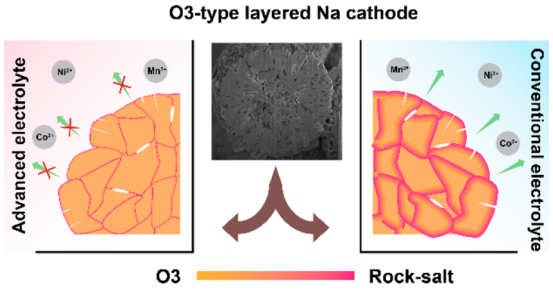
DISCLAIMER

This report was prepared as an account of work sponsored by an agency of the United States Government. Neither the United States Government nor any agency thereof, nor any of their employees, nor any of their contractors, subcontractors, or their employees, makes any warranty, express or implied, or assumes any legal liability or responsibility for the accuracy, completeness, or any third party's use or the results of such use of any information, apparatus, product, or process disclosed, or represents that its use would not infringe privately owned rights. Reference herein to any specific commercial product, process, or service by trade name, trademark, manufacturer, or otherwise, does not necessarily constitute or imply its endorsement, recommendation, or favoring by the United States Government or any agency thereof or its contractors or subcontractors. The views and opinions of authors expressed herein do not necessarily state or reflect those of the United States Government or any agency thereof.

Controlling Surface Phase Transition and Chemical Reactivity of O3-Layered Metal Oxide Cathodes for High-Performance Na-Ion Batteries

Junhua Song, Kuan Wang, Jianming Zheng, Mark H. Engelhard, Biwei Xiao, Enyuan Hu, Zihua Zhu, Chongmin Wang, Manling Sui, Yuehe Lin, David Reed, Vincent L. Sprenkle, Pengfei Yan, and Xiaolin Li

ABSTRACT: O3-layered metal oxides are promising cathode materials for high-energy Na-ion batteries (SIBs); however, they suffer from fast capacity fade. Here, we develop a high-performance O3-Na-$Ni_{0.68}Mn_{0.22}Co_{0.10}O_2$ cathode for SIBs toward practical applications by suppressing the formation of a rock salt layer at the cathode surface with an advanced electrolyte. The cathode can deliver a high specific capacity of ~196 mAh g^{-1} and demonstrates >80% capacity retention over 1000 cycles. $NaNi_{0.68}Mn_{0.22}Co_{0.10}O_2$–hard carbon full-cells with practical loading (>2.5 mAh cm^{-2}) and lean electrolyte (~40 μL) demonstrate ~82% capacity retention after 450 cycles. A 60 mAh single-layer pouch cell has also been fabricated and demonstrated stable performance. This work represents a significant leap in SIB development and brings new insights to the development of advanced layered metal oxide cathodes for alkaline-ion batteries.



Sodium-ion batteries (SIBs), with the intrinsic advantages of resource abundance and geographic uniformity, are desired alternative battery technology to Li-ion batteries (LIBs) for grid-scale energy storage and transportation applications.[1−3] To make SIBs comparable to LIBs in electrochemical performance, it is essential to develop advanced cathode materials of high capacity and long cycle life. Among the recent efforts made in this regard,[4−10] the O3-type layered transition-metal oxides (O3-NaTMOs) with high specific capacity, tunable transition metal composition/secondary particle structure, and high tap density are expected as promising candidate cathodes toward practical applications.[3,11−18] However, the nickel-rich O3-NaTMOs suffer from irreversible phase transition at high voltage and limited cycle life, similar to their Li analogues, if not even worse.[19−23] Approaches such as nanostructure design, elemental doping, and surface coating have been developed to synthesize high-performance O3-NaTMOs cathodes for practical applications. Recently, the radially aligned gradient structured O3-$NaNi_{0.6}Co_{0.05}Mn_{0.35}O_2$ has demonstrated ~157 mAh g^{-1} specific capacity at 15 mA g^{-1} in half-cells and 125 mAh g^{-1} with 80% retention over 300 cycles in full-cells.[14] Ti doping and MgO surface coating have been used to mitigate cation mixing, electrolyte penetration, and intragranular cracking.[15,16] Cu/Fe substitution and TiO_2 interphase construction have been demonstrated to be effective in alleviating the irreversible extraction of Na^+ from their octahedral position and hence reduce the destructive impact on the layered structure.[17,18] However, the electrochemical performance of O3-NaTMOs is still far from satisfactory for industrial applications.[21−23]

Interface stability, particularly the structural and chemical stability, is known to be essential for battery performance.[24,25] In the development of LIBs, electrolyte optimization and electrode surface engineering are classic protocols for controlling the formation of solid electrolyte interphase (SEI), cathode electrolyte interphase (CEI), and electrode surface structure/chemistry.[26−32] However, these strategies

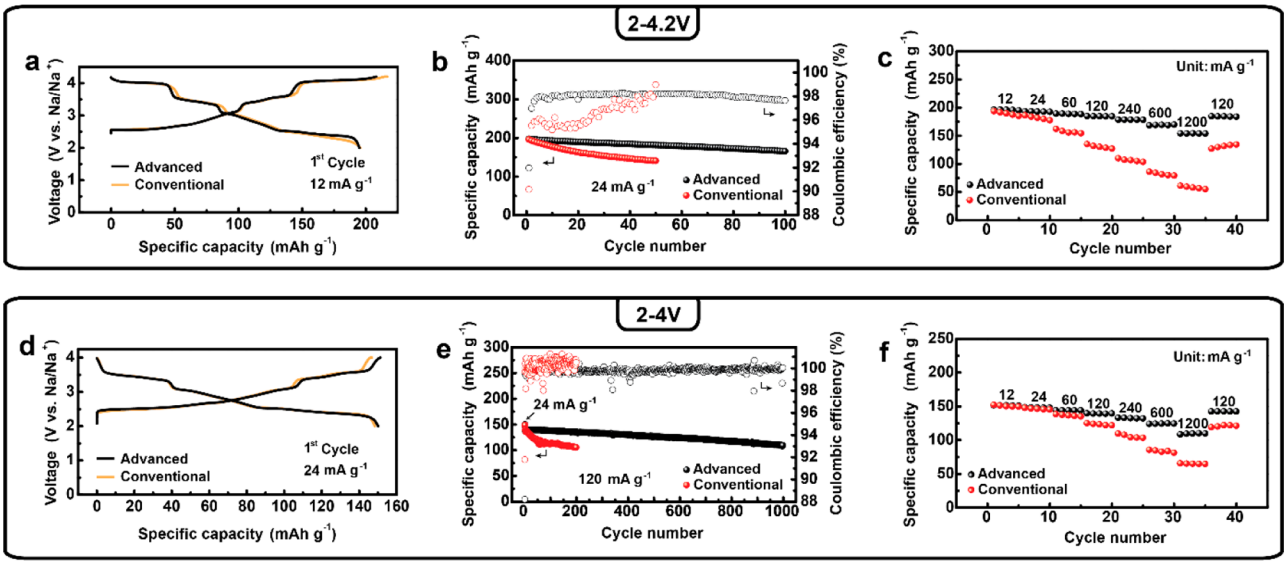


Figure 1. Electrochemical performance of O3-NaNMC682210 in half-cells. (a–c) Electrochemical performance between 2 and 4.2 V in advanced and conventional electrolyte. (a) First cycle charge–discharge curves. (b) Long-term cycling at 24 mA g^{-1}. (c) Performance at different current densities. (d–f) Electrochemical performance between 2 and 4 V in advanced and conventional electrolyte. (d) First cycle charge–discharge curves. (e) Long-term cycling at 120 mA g^{-1}. (f) Performance at different current densities.

have not been systematically studied on SIB cathodes. Here, we demonstrate a long-life O3-type layered $NaNi_{0.68}Mn_{0.22}Co_{0.10}O_2$ (O3-NaNMC682210) cathode for practical SIBs by controlling the surface phase transition and interphase stability. The O3-NaNMC682210 cathode, by suppressing the propagation of surface rock salt layer with localized high-concentration electrolyte,[27] delivers a specific capacity of ~196 mAh g^{-1}, a specific energy of ~612 Wh kg^{-1} (based on the cathode), and >83% capacity retention over 100 cycles between 2 and 4.2 V (vs Na/Na^+). The cathode has ~80% capacity retention over 1000 cycles with a specific capacity of ~151 mAh g^{-1} between 2 and 4 V. The good cathode reversibility is consistently confirmed by the O3-NaNMC682210–hard carbon full-cells with ~81% capacity retention over 1000 cycles. Full-cells with practical loading (>2.5 mAh cm^{-2}) and controlled electrolyte amount (~40 μL) also have been demonstrated. The capacity retention is >82% after 450 cycles. A 60 mAh single-layer pouch cell has also been fabricated and demonstrated stable performance. This work is a momentous step forward in developing high-performance SIBs. It unravels the indispensable role of controlling the surface phase transition in maximizing the cathode structure stability and battery performance and provides general guidance for improving the performance of layered metal oxide cathodes for Li/Na-ion batteries.

O3-NaNMC682210 was selected as the cathode material based on the overall electrochemical performance and cost balance.[33–35] It was prepared via careful control of the synthesis parameters of the coprecipitation-annealing approach (see Experimental Section and Supplementary Note 1 in the Supporting Information). SEM analysis shows that the spherical O3-NaNMC682210 secondary particles are ~10 μm in diameter consisting of densely packed primary particles (Figure S1). The detailed characterizations of the cathode composition, structure, and NMC682210 precursor are shown in Figures S1–S4.

The electrochemical performance of O3-NaNMC682210 was evaluated in half-cells using both carbonate-based electrolyte (1 M $NaPF_6$ in ethylene carbonate (EC)/dimethyl carbonate (DMC) (30/70) with 2 wt % fluoroethylene carbonate (FEC), noted as conventional throughout the Letter) and our localized high-concentration ether-based electrolyte (1.2 M NaFSI in dimethoxyethane (DME) with (bis(2,2,2-trifluoroethyl) ether (BTFE), noted as advanced throughout the Letter) (Figure 1). The first cycle charge–discharge curves and specific capacities are similar in both electrolytes in either voltage window of 2–4.2 or 2–4 V (Figure 1a,d). At low current density of 12 mA g^{-1}, the specific capacity is ~196 mAh g^{-1} (2–4.2 V) and ~151 mAh g^{-1} (2–4 V), respectively. They correspond to specific energy densities of 421 Wh kg^{-1} (2–4 V) and 612 Wh kg^{-1} (2–4.2 V) based on the cathode, very close to some LIB chemistries.[36,37]

The cycling stability and rate capability show substantial improvements switching from conventional electrolyte to the advanced system. Between 2 and 4.2 V, the O3-NaNMC682210 cathode delivers good cycling stability with ~83% capacity and specific energy retention after 100 cycles at 24 mA g^{-1} in the advanced electrolyte, contrasting to the 72% after 50 cycles in the conventional electrolyte (Figures 1b and S5a). The specific capacity at high current density of 1200 mA g^{-1} is 155 mAh g^{-1} in the advanced electrolyte, ~3 times the value (55 mAh g^{-1}) obtained in the conventional counterpart (Figure 1c). For cells tested between 2 and 4 V, the cathode demonstrates ~80% capacity and energy retention over 1000 cycles at 120 mA g^{-1} in the advanced electrolyte, while the capacity retention is only 75% after 200 cycles in the conventional system (Figures 1e and S5b). The Coulombic efficiency of the conventional electrolyte has large fluctuation, indicating heavy decomposition of the electrolyte. The good cycling performance of O3-NaNMC682210 in the advanced electrolyte has actually been observed at various current densities. In particular, the capacity retention at 600 mA g^{-1} is ~85% over 2000 cycles (Figure S6). The rate performance shows that the specific capacity at 1200 mA g^{-1} is 110 mAh g^{-1}, ~2 times the value (65 mAh g^{-1}) achieved in the conventional electrolyte (Figure 1f).

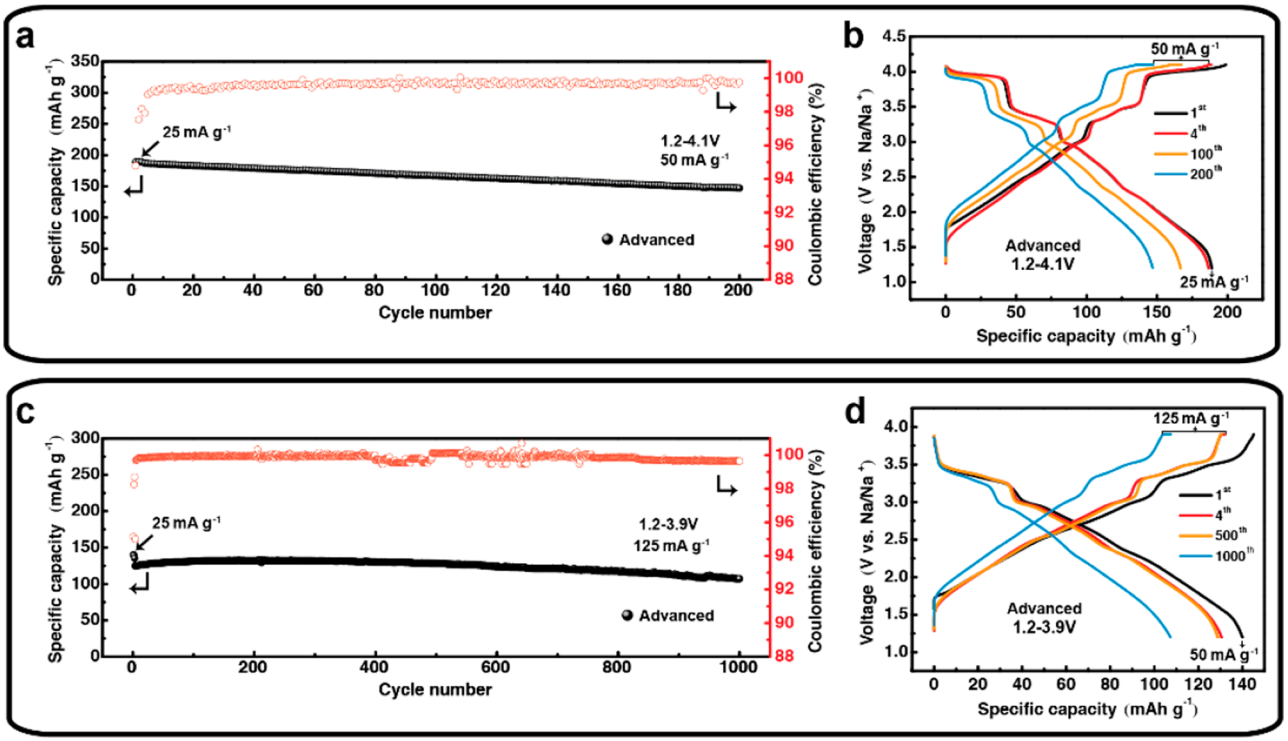


Figure 2. Electrochemical performance of O3-NaNMC682210−hard carbon full-cells. (a and b) Cycling performance (a) and charge−discharge curves (b) in the voltage range of 1.2−4.1 V. (c and d) Cycling performance (c) and charge−discharge curves (d) in the voltage range of 1.2−3.9 V.

Ex situ XRD analyses and a close comparison of the charge−discharge curves at various cycles have been carried out to understand the mechanism of the different performance in the two electrolyte systems. At the first cycle, the cathode shows almost identical charge−discharge profiles (Figure 1) and the *ex situ* XRD exhibits similar phase transitions (Figure S7). In both electrolytes, the typical hexagonal O3 peaks, including (003), (101), and (107), gradually shift toward lower angle during desodiation, indicating the formation of monoclinic P3 structure (Figure S8) with increased interlayer spacing, and then almost fully recover to their original O3 positions during sodiation.[33] After long-term cycling, however, the charge−discharge curves and the corresponding dQ/dV plots exhibit big differences around several plateaus (Figure S9). Using the cathodes cycled between 2 and 4.2 V as an example, the differences are corroborated by the *ex situ* XRD analyses, which show much poorer phase reversibility after 50 cycles in the conventional electrolyte than in the advanced electrolyte (Figures S7, S10, and S11). The high-voltage plateau (4−4.2 V) that corresponds to the O3−P3 phase transition particularly shows decreased reversibility after cycling in the conventional electrolyte. After 50 cycles, ex situ XRD shows mainly O3 phase for the cathode cycled in the advanced electrolyte (full discharge state at 2 V), while a mixed O3−P3 phase is observed in the conventional electrolyte (full discharge state at 2 V). The mixed phase formation is believed to be associated with the severe surface phase transition, enlarged interlayer distance, and significant TM reduction−dissolution (*vide infra*).[38] The dQ/dV analyses of the O3-NaNMC682210 cycled in the two electrolytes reveal different kinetics at various voltage plateaus (Figures S12 and S13). In the voltage range of 2−4.2 V, the performance difference is mainly associated with the high-voltage plateau between 4 and 4.2 V. In the conventional electrolyte, the dQ/dV signal related to that plateau is greatly shortened or almost completely disappears with the rate increase (Figure S12). In contrast, the same dQ/dV signal remains similar in the advanced electrolyte with only a slightly reduced peak intensity at high rates (Figure S12). The dQ/dV curves of the cells cycled between 2 and 4 V exhibit similar phenomena, while the capacity loss is more associated with the plateau at ∼2.3 V (Figure S13).

The two electrolytes have similar ion conductivity (the ion conductivity of the advanced electrolyte actually is slightly lower than that of the conventional electrolyte), and the metal deposition at the anode side should not have significant dependence on the voltage plateaus.[27] Hence, the above results indicate that the drastically dissimilar cycling stability and rate performance are more related to the Na-ion transfer kinetics at the cathode side rather than the electrolyte effect on the Na metal side. To help differentiate the major cause for the capacity fade in the advanced electrolyte, a control experiment was carried out, in which a new Na metal was applied to an O3-NaNMC682210 half-cell after 50 cycles. The cell having similar fading trend after Na metal change corroborates that the capacity fade in this system is mainly from the cathode side, and the effects from Na metal and electrolyte conductivity are minimum (Figure S14). Three-electrode electrochemical impedance spectroscopy (EIS) tests (Supplementary Note 2) show significant cathode impedance increase for the cells with the conventional electrolyte and hence further corroborate that the cathode determines the performance decay (Figure S15). It is believed that the improved cycling and rate performance in the advanced electrolyte is related to the mitigated surface phase transition and hence lower cathode impedance compared to that in the conventional electrolyte (*vide infra*). Full-cell test and post-mortem analyses of the cathode have

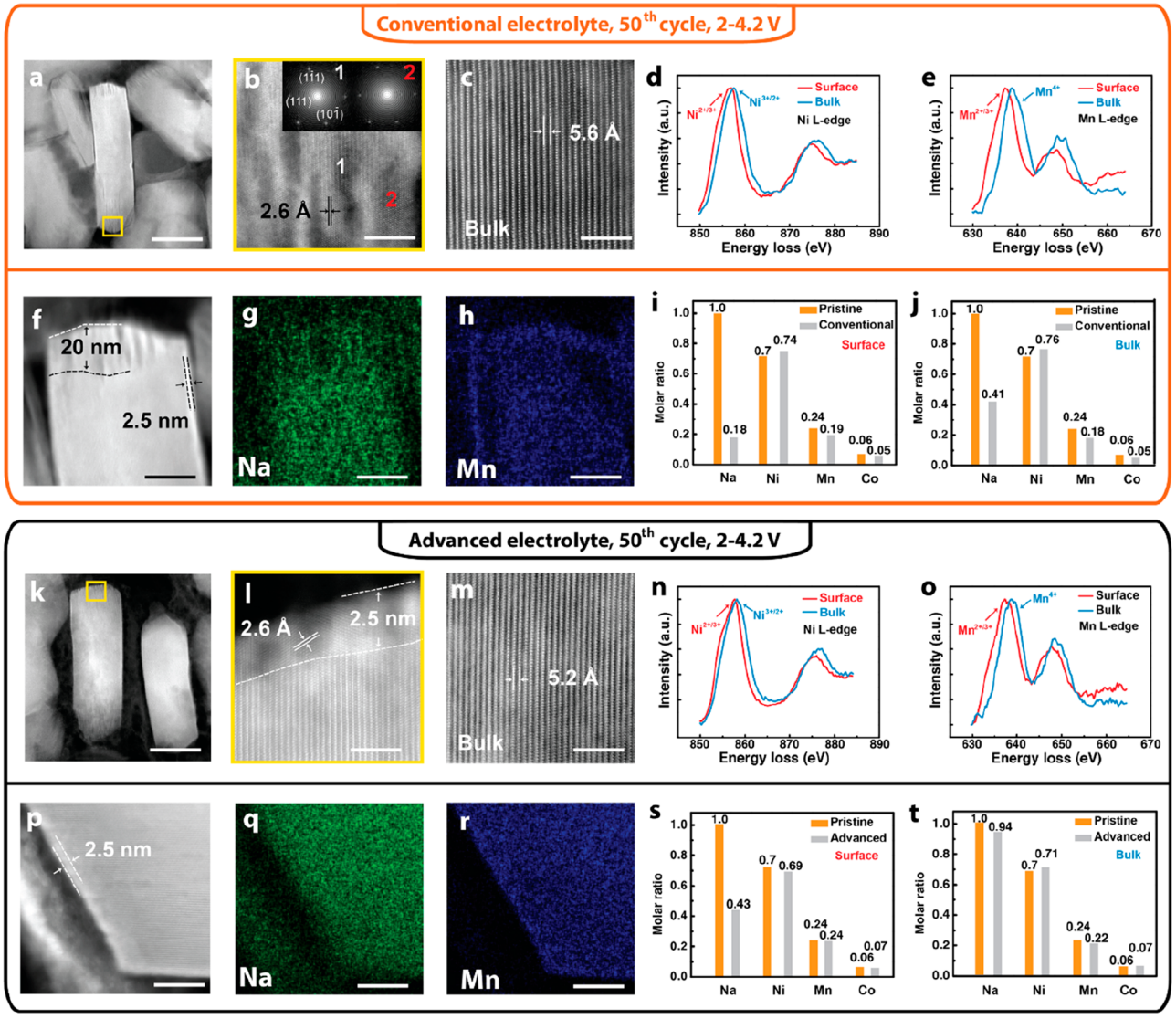


Figure 3. Characterization of the surface phase transition layer of O3-NaNMC682210 cathodes after 50 cycles between 2 and 4.2 V. (a–j) Conventional electrolyte. (a) Typical low-magnification STEM-HAADF image. (b) HAADF image taken at the surface region of the primary particle marked with the yellow box in panel a. Inset are the FFT taken at numbered regions. (c) HAADF image taken at the bulk region of a primary particle. (d and e) Typical EELS analysis of Ni L-edge (d) and Mn L-edge (e). (f) Zoom-in STEM-HAADF image of panel a. (g and h) EDS mappings of Na and Mn of the particle in panel f. (i and j) Chemical composition change of the surface (i) and bulk (j) of a primary particle. (k–t) Advanced electrolyte. (k) Typical low-magnification STEM-HAADF image. (l) HAADF image taken at the surface region of the primary particle marked with the yellow box in panel k. (m) HAADF image taken at the bulk region of a primary particle. (n and o) EELS analysis of Ni L-edge (n) and Mn L-edge (o). (p) Zoom-in STEM-HAADF image. (q and r) EDS mappings of Na and Mn of the particle in panel p. (s and t) Chemical composition change of the surface (s) and bulk (t) of a primary particle. Scale bar: 100 nm (a and k), 4 nm (b and c; i–m), 20 nm (f–h and p–r).

been performed to further verify the hypothesis and understand the mechanism of the enhanced cycling stability in the advanced electrolyte.

O3-NaNMC682210–hard carbon full-cells were tested to completely avoid the interference from Na metal. The rate performance of the hard carbon anode was first performed in half-cells as the reference for full-cell balancing (Figure S16). Hard carbon in convention and advanced electrolyte show similar specific capacity of ~200 mAh g^{-1} and good cycling stability with ~93% capacity retention over 100 cycles (Figure S17). The full-cells then were assembled by matching the cathodes with precycled hard carbon anodes at the n/p ratio of 1.1:1 (see Experimental Section in the Supporting Information). Figure 2 presents the excellent cycling performance of the full-cells with advanced electrolyte. A specific capacity of 188 mAh g^{-1} (based on the cathode) was obtained at 25 mA g^{-1} between 1.2 and 4.1 V. It is very close to the capacity of O3-NaNMC682210 cathode in half-cells. It also has demonstrated good cycling stability with capacity retention of ~80% over 200 cycles at 50 mA g^{-1} (Figure 2 a,b). The full-cell cycled between 1.2 and 3.9 V delivers a specific capacity of 137 mAh g^{-1} (based on cathode) at 25 mA g^{-1} and 129 mAh g^{-1} at 125 mA g^{-1} (Figure 2c). The cycling stability is even better than that of half-cells (Figure 1e) with ~81% capacity retention over 1000 cycles (Figure 2 c,d). Although the fundamental mechanism of the good cycling stability of full-cells is not fully understood, it is believed that precycled hard carbon anodes are beneficial for more stable SEI than Na metal

and reduce gas formation at the cathode.[39] The full-cells also have good rate performance in both voltage ranges. The discharge capacity at large current density of 500 mA g^{-1} is ~161 mAh g^{-1} between 1.2 and 4.1 V and 110 mAh g^{-1} between 1.2 and 3.9 V (Figure S18).

The cyclability and rate performance are poor for full-cells with the conventional electrolyte (Figure S19). The long-term cycling shows capacity retention of ~52% over 100 cycles between 1.2 and 4.1 V (Figure S19a) and ~73% over 200 cycles between 1.2 and 3.9 V (Figure S19d). The full-cell tests not only corroborate that the cathode side improvement is mainly responsible for the enhanced electrochemical performance of half-cells with advanced electrolyte but also show that the advanced electrolyte is good for both O3-layered cathodes and hard carbon anodes.

Thorough post-mortem characterizations were conducted on the cycled O3-NaNMC682210 electrodes to understand the electrochemical performance differences. The cathodes after 50 cycles (discharge state, 2.0 V vs Na/Na^+) in the two electrolytes between 2 and 4.2 V were chosen as model systems. Side-by-side comparisons of the scanning transmission electron microscopy (STEM) analyses of the surface transition layer show that the cycled O3-NaNMC682210 in the conventional electrolyte (Figure 3a–j) has many more structural and chemical changes than in the advanced electrolyte (Figure 3k–t). In terms of thickness, the phase transition layer at the surface perpendicular to the (003) transition metal (TM) layer is ~20 nm thick in the conventional electrolyte (Figure 3a,f), much larger than the 2–3 nm in the advanced electrolyte (Figure 3k,i,p). High-angle annular dark-field (HAADF) images (Figure 3b,i) and the fast Fourier transform (FFT, inset of Figure 3b) patterns show that the transitioned surface layer has a typical rock salt structure with a lattice distance of ~2.6 Å, contrasting to the layered structure underneath. It is also intriguing to note that the surface transition layer is anisotropic along or perpendicular to the TM layers. Unlike the large thickness difference in the perpendicular direction, it has similar thickness of 2–3 nm at the surface parallel to the (003) plane in both electrolytes (Figure 3f,p). This is consistent with the fact that the direction perpendicular to the TM layers has repeated ion shuttling. The finding provides insights for more effective surface doping or engineering toward layered cathodes of better cyclability.

The contrasting surface phase transitions after cycling in the two electrolytes are not limited to the structural change. Energy-dispersive X-ray spectroscopy (EDS) and electron energy loss spectroscopy (EELS) studies reveal significantly different chemical compositions and valence states of the TMs in the surface phase transition layer (Figure 3d,e,g–j,n,o,q–t). In the conventional electrolyte, the cycled cathode surface has apparent Na deficiency, Mn dissolution, and reduction of TMs (Figures 3d,e,g–j, S20a–c, and S21a), compared to the pristine cathode (Figures S1 and S22). This is consistent with the capacity fade, increased bulk lattice distance to ~5.6 Å (Figure 3c), and poor phase reversibility upon repeated cycling in the conventional electrolyte (Figure S11).[24,40,41] In contrast, the cycled cathode in the advanced electrolyte has similar bulk phase to the pristine sample with only a thin surface phase transition layer showing Na deficiency and reduction of TMs (Figures 3n,o,q–t, S20d–f, and S21b). It corroborates the good electrochemical capacity retention, similar bulk lattice distance to the pristine cathode of ~5.2 Å (Figure 3m), and reversible phase change upon long-term charge–discharge (Figure S10). The changes of the surface TMs' valence also are verified by X-ray photoelectron spectroscopy (XPS) study. The Ni^{3+}/Ni^{2+} ratio of cycled cathode in the advanced electrolyte is ~2.1 times that in the conventional electrolyte (Figure S23). Considering the reduced surface TMs are more susceptible to dissolution into electrolyte and deposition on the opposite electrode,[42] XPS analyses of the TMs on counter electrodes also were investigated for both cycled half-cells and full-cells. Stronger Ni 2p signals were detected on the Na metals and hard carbon anodes cycled in the conventional electrolyte than in the advanced electrolyte (Figure S24).

Figures S25 and S26 are the TEM images and XPS spectra of typical CEI developed in the two electrolyte systems. Similar to LIBs, the CEI does not uniformly cover the SIB cathodes.[31] For many areas we have checked, the CEI thickness in the conventional electrolyte (~4 nm) is thicker than that obtained in the advanced electrolyte (~3 nm) (Figure S25). The C 1s and F 1s XPS spectra also show some differences between the CEI compositions (Figure S26), consistent with the literature using similar salt and electrolyte systems.[30] The intragranular cracking, which has been regarded as a major fading mechanism for layered metal oxides in LIBs and SIBs, also has been investigated.[14,20,43,44] The values for the number of cracks per unit area of the cycled cathodes in both electrolytes are very close to each other, and there seems to be slightly more cracking observed for the cathode cycled in the advanced electrolyte (Figure S27).

The above analyses clearly show that the controlled surface phase transition is the determining factor for the superb electrochemical performance of O3-NaNMC682210 in the advanced electrolyte, while CEI, intragranualr cracking, and the surface phase transition layer all contribute to the electrochemical performance fade.[45–47] It is believed that the thicker CEI from the increased deposition of the electrolyte decomposition products on the cathode surface impedes Li penetration to the cathode and leads to a reduced kinetics in the bulk. The Na deficiency, Mn dissolution, and reduction of transition metals are related to the electrolyte interaction with cathode surface. Gassing, as one result of the parasitic reactions at the interphase, is believed to be another possible reason for uneven current distribution and heterogeneity of the cathode and hence contributes to the noisy Coulombic efficiency, cathode structural change, and capacity fade in the conventional electrolyte.[39,48]

Based on the EIS result and the above TEM and XPS analyses, our current understanding/hypothesis is that the surface phase transition and the formation and evolution of rock salt layer are the main decisive reasons for the impedance increase. It works together with the cracking, metal dissolution, CEI, *etc.*, leading to the cathode structure and capacity fade. Mitigation of continuous formation of the cathode rock salt layer (1) alleviates the loss of the layer structured active cathode material, (2) controls the increase of impedance, (3) maintains the transition metal valence state, and (4) reduces the transition metal dissolution. This is one step further toward understanding the fading mechanism and boosting the performance of Ni-rich O3-NaNMC682210 cathode, although the molecular mechanism of the surface phase transition layer evolution requires further investigation.

With the surface phase transition and chemical reactivity well-controlled, high-performance SIB full-cells have been demonstrated with practical loading O3-NaNMC682210 cathodes, hard carbon anodes, and controlled amount of

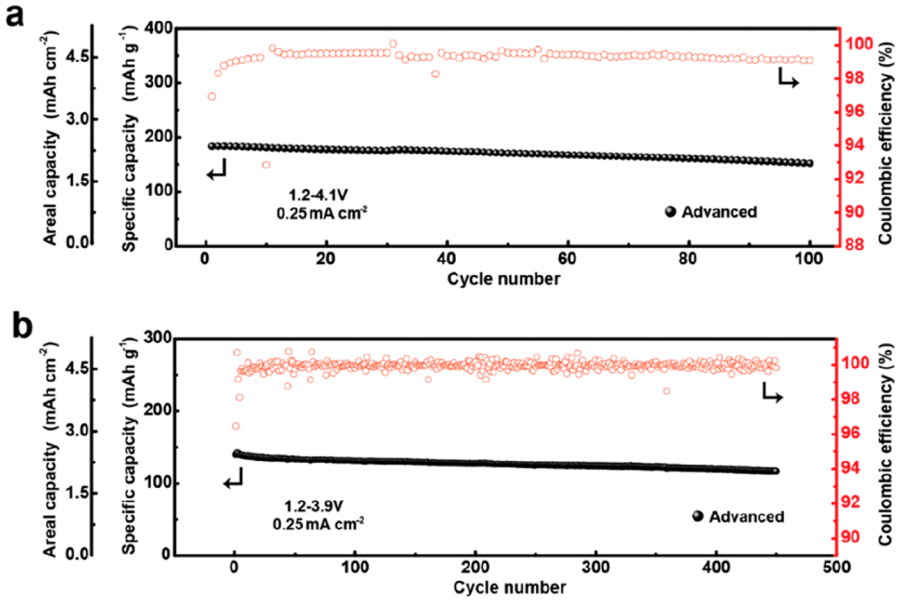


Figure 4. Long-term cycling stability of O3-NaNMC682210−hard carbon full-cells with practical loading and lean advanced electrolyte. (a) Cycling stability between 1.2 and 4.1 V. (b) Cycling stability between 1.2 and 3.9 V.

advanced electrolyte. The high loading hard carbon anodes also were precycled to alleviate the challenges from the low initial Coulombic efficiency. The full-cells were assembled with an n/p ratio of 1.1/1 and electrolyte amount of 40 μL. The ratio between the electrolyte amount and the cell capacity is reasonable for coin cell full-cells, even though it may be slightly high for practical large format cells. Figures 4 and S28 show the typical performance of full-cells with an areal capacity of ∼2.5 mAh cm^{-2}. At 0.25 mA cm^{-2}, high specific capacities of ∼184 mAh g^{-1} and 141 mAh g^{-1} (based on cathode) were obtained for full-cells cycled in the voltage ranges of 1.2−4.1 V and 1.2−3.9 V, respectively. These values are very close to what have been acquired in the half-cells and low loading full-cells with flooded electrolyte. The full-cell shows good cycling stability in the voltage range of 1.2−4.1 V. The capacity retention after 100 cycles is ∼83% (Figure 4a). The full-cell cycled between 1.2 and 3.9 V delivers even better cycling stability with >82% capacity retention over 450 cycles (Figure 4b).

It is very encouraging that the estimated specific energy of the full-cell between 1.2 and 4.1 V achieves ∼290 Wh kg^{-1} based on the total mass of cathode and anode, and the energy retention is 80% (Figure S29). The cell-level specific energy would be ∼160 Wh kg^{-1} if we extrapolate to practical large-format cells using the optimized LIB design with 55 wt % active materials (Argonne BatPac Version 3.1).[49] This value is already competitive with the commercial $LiFePO_4$−graphite batteries (156 Wh kg^{-1})[34] and attractive to applications, including low-speed vehicles and stationary storage systems. The practical prospect was further demonstrated with a 60 mAh single-layer pouch cell in the voltage range of 1.2−3.9 V, which retains ∼95% of the capacity over 100 cycles (Figure S30).

In summary, we have unravelled the essentials of the surface phase transition in enabling long-life O3-layered metal oxide cathodes. High-performance SIBs O3-NaNMC682210 cathode and advanced electrolyte have been demonstrated in a full-cell configuration and close-to-practice design parameters (Table S1). The full-cell performance can be further promoted by integrating advanced anode materials and an even better electrolyte. Our strategies are general and have been demonstrated to be applicable for other O3-type NaTMO cathodes (Figure S31). This work paves a new way toward practical SIBs, and the fundamental insights shed light on the development of future cobalt-free/low-cobalt cathode materials in Li-ion batteries and other battery chemistries.

AUTHOR INFORMATION

Corresponding Authors

Jianming Zheng − *Pacific Northwest National Laboratory, Richland, Washington 99352, United States*; Email: xmzhjm@126.com

Yuehe Lin − *School of Mechanical and Materials Engineering, Washington State University, Pullman, Washington 99164, United States*; orcid.org/0000-0003-3791-7587; Email: yuehe.lin@wsu.edu

Pengfei Yan − *Beijing Key Laboratory of Microstructure and Properties of Solids, Institute of Microstructure and Properties of Advanced Materials, Beijing University of Technology, Beijing 100124, China*; orcid.org/0000-0001-6387-7502; Email: pfyan@bjut.edu.cn

Xiaolin Li − *Pacific Northwest National Laboratory, Richland, Washington 99352, United States*; orcid.org/0000-0002-7728-0157; Email: xiaolin.li@pnnl.gov

Authors

Junhua Song − *Pacific Northwest National Laboratory, Richland, Washington 99352, United States; School of Mechanical and Materials Engineering, Washington State University, Pullman, Washington 99164, United States*

Kuan Wang − *Beijing Key Laboratory of Microstructure and Properties of Solids, Institute of Microstructure and Properties of Advanced Materials, Beijing University of Technology, Beijing 100124, China*
Mark H. Engelhard − *Pacific Northwest National Laboratory, Richland, Washington 99352, United States;* orcid.org/0000-0002-5543-0812
Biwei Xiao − *Pacific Northwest National Laboratory, Richland, Washington 99352, United States*
Enyuan Hu − *Chemistry Division, Brookhaven National Laboratory, Upton, New York 11973, United States;* orcid.org/0000-0002-1881-4534
Zihua Zhu − *Pacific Northwest National Laboratory, Richland, Washington 99352, United States;* orcid.org/0000-0001-5770-8462
Chongmin Wang − *Pacific Northwest National Laboratory, Richland, Washington 99352, United States;* orcid.org/0000-0003-3327-0958
Manling Sui − *Beijing Key Laboratory of Microstructure and Properties of Solids, Institute of Microstructure and Properties of Advanced Materials, Beijing University of Technology, Beijing 100124, China*
David Reed − *Pacific Northwest National Laboratory, Richland, Washington 99352, United States*
Vincent L. Sprenkle − *Pacific Northwest National Laboratory, Richland, Washington 99352, United States*

Complete contact information is available at: https://pubs.acs.org/10.1021/acsenergylett.0c00700

Author Contributions

[⊥]J.S. and K.W. contributed equally to this work.

Notes

The authors declare no competing financial interest.

■ ACKNOWLEDGMENTS

X.L. acknowledges the financial support from the U.S. Department of Energy's (DOE's) Office of Electricity under Contract No. 70247A. P.Y. thanks the National Natural Science Fund for Innovative Research Groups (Grant No. 51621003) and the National Key Research and Development Program of China (Grant No. 2016YFB0700700). Y.L. acknowledges the support from the start-up funds from Washington State University. Some of the microscopic and spectroscopic characterizations were conducted in the William R. Wiley Environmental Molecular Sciences Laboratory (EMSL), a national scientific user facility located at PNNL, which is sponsored by the DOE Office of Biological and Environmental Research (BER). The authors also are grateful for the cathode precursor material provided by the project supported by the Assistant Secretary for Energy Efficiency and Renewable Energy, Office of Vehicle Technologies of the U.S. Department of Energy under Contract No. DE-AC02-05CH11231, Subcontract No. 18769 and No. 6951379 under the Advanced Battery Materials Research (BMR) program.

■ REFERENCES

(1) Vaalma, C.; Buchholz, D.; Weil, M.; Passerini, S. A cost and resource analysis of sodium-ion batteries. *Nat. Rev. Mater.* **2018**, *3*, 18013.
(2) Turcheniuk, K.; Bondarev, D.; Singhal, V.; Yushin, G. Ten years left to redesign lithium-ion batteries. *Nature* **2018**, *559*, 467−470.
(3) Bauer, A.; Song, J.; Vail, S.; Pan, W.; Barker, J.; Lu, Y. The scale-up and commercialization of nonaqueous Na-ion battery technologies. *Adv. Energy Mater.* **2018**, *8*, 1702869.
(4) Yabuuchi, N.; Kajiyama, M.; Iwatate, J.; Nishikawa, H.; Hitomi, S.; Okuyama, R.; Usui, R.; Yamada, Y.; Komaba, S. P2-type $Na_x[Fe_{1/2}Mn_{1/2}]O_2$ made from earth-abundant elements for rechargeable Na batteries. *Nat. Mater.* **2012**, *11*, 512−517.
(5) Park, Y. U.; Seo, D. H.; Kwon, H. S.; Kim, B.; Kim, J.; Kim, H.; Kim, I.; Yoo, H. I.; Kang, K. A new high-energy cathode for a Na-ion battery with ultrahigh stability. *J. Am. Chem. Soc.* **2013**, *135*, 13870−13878.
(6) Barpanda, P.; Oyama, G.; Nishimura, S. I.; Chung, S. C.; Yamada, A. A 3.8-V earth-abundant sodium battery electrode. *Nat. Commun.* **2014**, *5*, 4358.
(7) Lee, H. W.; Wang, R. Y.; Pasta, M.; Lee, S. W.; Liu, N.; Cui, Y. Manganese hexacyanomanganate open framework as a high-capacity positive electrode material for sodium-ion batteries. *Nat. Commun.* **2014**, *5*, 5280.
(8) Wang, L.; Song, J.; Qiao, R.; Wray, L. A.; Hossain, M. A.; Chuang, Y.-D.; Yang, W.; Lu, Y.; Evans, D.; Lee, J. J.; Vail, S.; Zhao, X.; Nishijima, M.; Kakimoto, S.; Goodenough, J. B. Rhombohedral prussian white as cathode for rechargeable sodium-ion batteries. *J. Am. Chem. Soc.* **2015**, *137*, 2548−2554.
(9) Rong, X.; Hu, E.; Lu, Y.; Meng, F.; Zhao, C.; Wang, X.; Zhang, Q.; Yu, X.; Gu, L.; Hu, Y. S.; Li, H.; Huang, X.; Yang, X. Q.; Delmas, C.; Chen, L. Anionic redox reaction-induced high-capacity and low-strain cathode with suppressed phase transition. *Joule* **2019**, *3*, 612.
(10) Maitra, U.; House, R. A.; Somerville, J. W.; Tapia-Ruiz, N.; Lozano, J. G.; Guerrini, N.; Hao, R.; Luo, K.; Jin, L.; Pérez-Osorio, M. A.; Massel, F.; Pickup, D. M.; Ramos, S.; Lu, X.; McNally, D. E.; Chadwick, A. V.; Giustino, F.; Schmitt, T.; Duda, L. C.; Roberts, M. R.; Bruce, P. G. Oxygen redox chemistry without excess alkali-metal ions in $Na_{2/3}[Mg_{0.28}Mn_{0.72}]O_2$. *Nat. Chem.* **2018**, *10*, 288−295.
(11) Liu, H.; Xu, J.; Ma, C.; Meng, Y. S. A new O3-type layered oxide cathode with high energy/power density for rechargeable Na batteries. *Chem. Commun.* **2015**, *51*, 4693−4696.
(12) Deng, J.; Luo, W.; Lu, X.; Yao, Q.; Wang, Z.; Liu, H. K.; Zhou, H.; Dou, S. X. High energy density sodium-ion battery with industrially feasible and air-stable O3-type layered oxide cathode. *Adv. Energy Mater.* **2018**, *8*, 1701610.
(13) Sun, L.; Xie, Y.; Liao, X. Z.; Wang, H.; Tan, G.; Chen, Z.; Ren, Y.; Gim, J.; Tang, W.; He, Y. S.; Amine, K.; Ma, Z. F. Insight into Ca-substitution effects on O3-type $NaNi_{1/3}Fe_{1/3}Mn_{1/3}O_2$ cathode materials for sodium-ion batteries application. *Small* **2018**, *14*, 1704523.
(14) Hwang, J. Y.; Oh, S. M.; Myung, S. T.; Chung, K. Y.; Belharouak, I.; Sun, Y. K. Radially aligned hierarchical columnar structure as a cathode material for high energy density sodium-ion batteries. *Nat. Commun.* **2015**, *6*, 6865.
(15) Hwang, J. Y.; Yu, T. Y.; Sun, Y. K. Simultaneous MgO coating and Mg doping of Na $[Ni_{0.5}Mn_{0.5}]O_2$ cathode: facile and customizable approach to high-voltage sodium-ion batteries. *J. Mater. Chem. A* **2018**, *6*, 16854−16862.
(16) Yao, H. R.; Wang, P. F.; Gong, Y.; Zhang, J.; Yu, X.; Gu, L.; Ouyang, C.; Yin, Y. X.; Hu, E.; Yang, X. Q.; Stavitski, E.; Guo, Y. G.; Wan, L. J. Designing air-stable O3-type cathode materials by combined structure modulation for Na-ion batteries. *J. Am. Chem. Soc.* **2017**, *139*, 8440−8443.
(17) Mu, L.; Xu, S.; Li, Y.; Hu, Y. S.; Li, H.; Chen, L.; Huang, X. Prototype sodium-ion batteries using an air-stable and Co/Ni-free O3-layered metal oxide cathode. *Adv. Mater.* **2015**, *27*, 6928.
(18) Guo, S.; Li, Q.; Liu, P.; Chen, M.; Zhou, H. Environmentally stable interface of layered oxide cathodes for sodium-ion batteries. *Nat. Commun.* **2017**, *8*, 135.
(19) Lin, F.; Markus, I. M.; Nordlund, D.; Weng, T. C.; Asta, M. D.; Xin, H. L.; Doeff, M. M. Surface reconstruction and chemical evolution of stoichiometric layered cathode materials for lithium-ion batteries. *Nat. Commun.* **2014**, *5*, 3529.

(20) Yan, P.; Zheng, J.; Gu, M.; Xiao, J.; Zhang, J. G.; Wang, C. M. Intragranular cracking as a critical barrier for high-voltage usage of layer-structured cathode for lithium-ion batteries. *Nat. Commun.* **2017**, *8*, 14101.
(21) Kim, J.; Lee, H.; Cha, H.; Yoon, M.; Park, M.; Cho, J. Prospect and reality of Ni-rich cathode for commercialization. *Adv. Energy Mater.* **2018**, *8*, 1702028.
(22) Kubota, K.; Komaba, S. Review-practical issues and future perspective for Na-ion batteries. *J. Electrochem. Soc.* **2015**, *162*, A2538−A2550.
(23) You, Y.; Manthiram, A. Progress in high-voltage cathode materials for rechargeable sodium-ion batteries. *Adv. Energy Mater.* **2018**, *8*, 1701785.
(24) Xu, K. Electrolytes and interphases in Li-ion batteries and beyond. *Chem. Rev.* **2014**, *114*, 11503−11618.
(25) Song, J.; Xiao, B.; Lin, Y.; Xu, K.; Li, X. Interphases in sodium-ion batteries. *Adv. Energy Mater.* **2018**, *8*, 1703082.
(26) Xiao, B.; Soto, F. A.; Gu, M.; Han, K. S.; Song, J.; Wang, H.; Engelhard, M. H.; Murugesan, V.; Mueller, K. T.; Reed, D.; Sprenkle, V. L.; Balbuena, P. B.; Li, X. Lithium-pretreated hard carbon as high-performance sodium-ion battery anodes. *Adv. Energy Mater.* **2018**, *8*, 1801441.
(27) Zheng, J.; Chen, S.; Zhao, W.; Song, J.; Engelhard, M. H.; Zhang, J. G. Extremely stable sodium metal batteries Enabled by Localized High-Concentration Electrolytes. *ACS Energy Lett.* **2018**, *3*, 315−321.
(28) Wang, J.; Yamada, Y.; Sodeyama, K.; Chiang, C. H.; Tateyama, Y.; Yamada, A. Superconcentrated electrolytes for a high-voltage lithium-ion battery. *Nat. Commun.* **2016**, *7*, 12032.
(29) Zheng, J.; Engelhard, M. H.; Mei, D.; Jiao, S.; Polzin, B. J.; Zhang, J. G.; Xu, W. Electrolyte additive enabled fast charging and stable cycling lithium metal batteries. *Nat. Energy* **2017**, *2*, 17012.
(30) Jiao, S.; Ren, X.; Cao, R.; Engelhard, M. H.; Liu, Y.; Hu, D.; Mei, D.; Zheng, J.; Zhao, W.; Li, Q.; Liu, N.; Adams, B. D.; Ma, C.; Liu, J.; Zhang, J. G.; Xu, W. Stable cycling of high-voltage lithium metal batteries in ether electrolytes. *Nat. Energy* **2018**, *3*, 739−746.
(31) Chen, S.; Zheng, J.; Mei, D.; Han, K. S.; Engelhard, M. H.; Zhao, W.; Xu, W.; Liu, J.; Zhang, J. G. High-voltage lithium-metal batteries enabled by localized high-concentration electrolytes. *Adv. Mater.* **2018**, *30*, 1706102.
(32) Fan, X.; Chen, L.; Borodin, O.; Ji, X.; Chen, J.; Hou, S.; Deng, T.; Zheng, J.; Yang, C.; Liou, S. C.; Amine, K.; Xu, K.; Wang, C. Non-flammable electrolyte enables Li-metal batteries with aggressive cathode chemistries. *Nat. Nanotechnol.* **2018**, *13*, 715.
(33) Hwang, J. Y.; Yoon, C. S.; Belharouak, I.; Sun, Y. K. A comprehensive study of the role of transition metals in O3-type layered $Na[Ni_xCo_yMn_z]O_2$ (x = 1/3, 0.5, 0.6, and 0.8) cathodes for sodium-ion batteries. *J. Mater. Chem. A* **2016**, *4*, 17952−17959.
(34) Myung, S. T.; Maglia, F.; Park, K. J.; Yoon, C. S.; Lamp, P.; Kim, S. J.; Sun, Y. K. Nickel-rich layered cathode materials for automotive lithium-ion batteries: achievements and perspectives. *ACS Energy Lett.* **2017**, *2*, 196−223.
(35) Zeng, X.; Zhan, C.; Lu, J.; Amine, K. Stabilization of a high-capacity and high-power nickel-based cathode for Li-ion batteries. *Chem.* **2018**, *4*, 690−704.
(36) Whittingham, M. S. History, evolution, and future status of energy storage. *Proc. IEEE* **2012**, *100*, 1518−1534.
(37) Whittingham, M. S. Ultimate limits to intercalation reactions for lithium batteries. *Chem. Rev.* **2014**, *114*, 11414−11443.
(38) Zheng, L.; Obrovac, M. N. Investigation of O3-type $Na_{0.9}Ni_{0.45}Mn_xTi_{0.55-x}O_2$ ($0 \leq x \leq 0.55$) as positive electrode materials for sodium-ion batteries. *Electrochim. Acta* **2017**, *233*, 284−291.
(39) Xia, J.; Petibon, R.; Xiao, A.; Lamanna, W. M.; Dahn, J. R. Some Fluorinated Carbonates as Electrolyte Additives for Li-$(Ni_{0.4}Mn_{0.4}Co_{0.2})O_2$/Graphite Pouch Cells. *J. Electrochem. Soc.* **2016**, *163*, A1637−A1645.
(40) Jung, S. K.; Gwon, H.; Hong, J.; Park, K. Y.; Seo, D. H.; Kim, H.; Hyun, J.; Yang, W.; Kang, K. Understanding the degradation mechanisms of $LiNi_{0.5}Co_{0.2}Mn_{0.3}O_2$ cathode material in lithium ion batteries. *Adv. Energy Mater.* **2014**, *4*, 1300787.
(41) Liu, W.; Oh, P.; Liu, X.; Lee, M. J.; Cho, W.; Chae, S.; Kim, Y.; Cho, J. Nickel-rich layered lithium transition-metal oxide for high-energy lithium-ion batteries. *Angew. Chem., Int. Ed.* **2015**, *54*, 4440−4457.
(42) Gilbert, J. A.; Shkrob, I. A.; Abraham, D. P. Transition metal dissolution, ion migration, electrocatalytic reduction and capacity loss in lithium-ion full cells. *J. Electrochem. Soc.* **2017**, *164*, A389−A399.
(43) Xia, S.; Mu, L.; Xu, Z.; Wang, J.; Wei, C.; Liu, L.; Pianetta, P.; Zhao, K.; Yu, X.; Lin, F.; Liu, Y. Chemomechanical interplay of layered cathode materials undergoing fast charging in lithium batteries. *Nano Energy* **2018**, *53*, 753−762.
(44) Yoon, C. S.; Park, K. J.; Kim, U. H.; Kang, K. H.; Ryu, H. H.; Sun, Y. K. High-energy Ni-rich $Li[Ni_xCo_yMn_{1-x-y}]O_2$ cathodes via compositional partitioning for next-generation electric vehicles. *Chem. Mater.* **2017**, *29*, 10436−10445.
(45) Zou, L.; Liu, Z.; Zhao, W.; Jia, H.; Zheng, J.; Yang, Y.; Wang, G.; Zhang, J. G.; Wang, C. Solid-liquid interfacial reaction trigged propagation of phase transition from surface into bulk lattice of Ni-rich layered cathode. *Chem. Mater.* **2018**, *30*, 7016−7026.
(46) Jarry, A.; Gottis, S.; Yu, Y.-S.; Roque-Rosell, J.; Kim, C.; Cabana, J.; Kerr, J.; Kostecki, R. The formation mechanism of fluorescent metal complexes at the $Li_xNi_{0.5}Mn_{1.5}O_{4-\delta}$/carbonate ester electrolyte interface. *J. Am. Chem. Soc.* **2015**, *137*, 3533−3539.
(47) Yan, P.; Zheng, J.; Liu, J.; Wang, B.; Cheng, X.; Zhang, Y.; Sun, X.; Wang, C.; Zhang, J. G. Tailoring grain boundary structures and chemistry of Ni-rich layered cathodes for enhanced cycle stability of lithium-ion batteries. *Nat. Energy* **2018**, *3*, 600−605.
(48) Krause, L. J.; Chevrier, V. L.; Jensen, L. D.; Brandt, T. The Effect of Carbon Dioxide on the Cycle Life and Electrolyte Stability of Li-Ion Full Cells Containing Silicon Alloy. *J. Electrochem. Soc.* **2017**, *164*, A2527−A2533.
(49) Nelson, P. A.; Gallagher, K. G.; Bloom, I. D.; Dees, D. W. *Modeling the performance and cost of lithium-ion batteries for electric-drive vehicles*;Argonne National Lab (ANL): Argonne, IL (United States), 2012.